Published in final edited form as:
Biochim Biophys Acta. 2013 October ; 1830(10): . doi:10.1016/j.bbagen.2013.05.015.

Osteotropic cancer diagnosis by an osteocalcin inspired molecular imaging mimetic

Jae Sam Lee[a,b,*] and **Ching-Hsuan Tung**[a,**]

Jae Sam Lee: jl2zt@virginia.edu; Ching-Hsuan Tung: CTung@tmhs.org

[a]Department of Translational Imaging, The Methodist Hospital Research Institute, Weill Medical College of Cornell University, Houston, TX 77030, USA

[b]Department of Radiology and Medical Imaging, School of Medicine, University of Virginia, Charlottesville, VA 22904, USA

Abstract

Background—Although microcalcifications of hydroxyapatite can be found in both benign and malignant osteotropic tumors, they are mostly seen in proliferative lesions, including carcinoma. The aim of this present study is to develop a molecular imaging contrast agent for selective identification of hydroxyapatite calcification in human osteotropic tumor tissues ex vivo and in human osteosarcoma cells in vitro.

Methods—A bioinspired biomarker, hydroxyapatite binding peptide (HABP), was designed to mimic natural protein osteocalcin property in vivo. A fluorescein isothiocyanate dye conjugated HABP (HABP-19) was utilized to characterize hydroxyapatite on human osteotropic tumor tissue sections ex vivo and to selectively image hydroxyapatite calcifications in human osteosarcoma cells in vitro.

Results—Using a HABP-19 molecular imaging probe, we have shown that it is possible to selectively image hydroxyapatite calcifications in osteotropic cancers ex vivo and in human SaOS-2 osteosarcoma cells in vitro.

Conclusion—Hydroxyapatite calcifications were selectively detected in osteotropic tissues ex vivo and in the early stage of the calcification process of SaOS-2 human osteosarcoma in vitro using our HABP-19 molecular imaging probe. This new target-selective molecular imaging probe makes it possible to study the earliest events associated with hydroxyapatite deposition in various osteotropic cancers at the cellular and molecular levels.

General significance—It potentially could be used to diagnose and treat osteotropic cancer or to anchor therapeutic agents directing the local distribution of desired therapy at calcified sites.

Keywords

Osteotropic; Calcification; Hydroxyapatite; Molecular imaging; Osteocalcin

[*]Correspondence to: J.S. Lee, Department of Radiology and Medical Imaging, School of Medicine, University of Virginia, Charlottesville, VA 22904, USA. Tel.: +1 434 243 8002. [**]Correspondence to: C.-H. Tung, Department of Translational Imaging, The Methodist Hospital Research Institute, Weill Medical College of Cornell University, 6565 Fannin, B5-008 Houston, TX 77030. Tel.: +1 713 441 8682.

Conflicts of interest statement
The authors declare no conflict of interest.

1. Introduction

Osteosarcoma (OS) is the most frequent type of primary malignant bone tumor that commonly affects adolescents and young adults with a high propensity for metastasis, predominantly to the lung, breast, kidney, and prostate cancers [1–3]. It is characterized as a highly cellular tumor composed of pleomorphic spindle-shaped cells capable of producing an osteoid matrix and it generally develops in the metaphyseal ends of long bones, within the medullary cavity, and penetrates the cortex of the bone to involve the surrounding soft tissue [4,5]. The American Cancer Society estimates that approximately 800 new cases of OS are diagnosed in the United States every year and about 400 of these are in children and teens. Despite effective primary tumor resection combined with neoadjuvant chemotherapy and conservative surgery, long-term survival rate is only 15–20% due to metastases, non-responsiveness to therapy, or disease relapse [6,7]. Early OS diagnosis would provide a great help for better understanding of the malignant bone tumor processes, however, poor diagnosis occurs in most patients because the mechanisms underlying the development, progression, and metastasis are mostly unknown and specific clinical symptoms are lacking in the early stages of the diseases [8–10].

The understanding of the complexity and heterogeneity of OS pathophysiology and metastasis requires the identification and detailed characterization of undefined regulators of OS and metastasis progression [11]. Histopathological subtypes of OS could include osteoblastic, chondroblastic, fibroblastic OS, and infrequent subtypes of telangiectatic and small cell OS [12]. Immunohistochemical analysis can be utilized for accurate diagnosis in undifferentiated OS and small round cell tumors arising in the bone. Protein osteocalcin (OCN) has been used for diagnostic purposes in the immunohistology because it is quite sensitive and specific to OS and exclusively expressed to several osteotropic tumors, including breast, ovarian, lung, brain, and prostate cancers [13–15]. OCN, a non-collagenous protein secreted by osteoblasts, is well known as a bone specific protein, which expression is closely related with bone formation through its ability to bind to the key mineral component of bone, hydroxyapatite (HA), with high affinity [16,17]. Moreover, OCN expression is believed to play an important role in the initiation and regulation of HA calcification [18]. The OCN affinity to HA is mainly attributed to highly conserved three -carboxyglutamic acid (Gla) residues. OCN remains unstructured in the absence of HA due to unfavorable negative charge interactions among Gla side chains, while interactions between Ca^{2+} on HA and dicarboxyl groups of Gla on OCN could induce a conformational change from random to α-helix, stabilizing the conserved region and conferring a high affinity for HA [17,19].

Pathological calcification, a process of insoluble calcium salt deposition primarily as HA, widely occurs in case of systemic mineral imbalance throughout the body [20–23]. Microcalcifications found in osteotropic tumors, mostly in breast and prostate cancers among others, are divided into two principle types of calcium salts, calcium oxalate (CO) and HA, based on their structure and chemical composition [24]. CO calcifications are mainly associated with benign disease and are rarely found in foci of carcinoma [25]. However, HA calcifications can be found in both benign and malignant lesions, although they are most often seen in proliferative lesions, including carcinoma [24–26]. Recently, we have developed a HA binding peptide (HABP-19) inspired from protein OCN that was used as a targeting imaging contrast for HA calcification in cardiovascular diseases and early osteoblastic activity [23,27]. In the present work we have used HABP-19 molecular imaging agent to validate HA calcification in osteotropic tumors (ex vivo) and human SaOS-2 cells (in vitro).

2. Materials and methods

FITC-labeled HABP-19 and the corresponding FITC-labeled control cHABP probes were prepared as previously described [27]. The sequences of HABP-19 and control cHABP are FITC-βAγEPRRγEVAγELγEPRRγEVAγEL-NH_2 and FITC-βAEPRREVAELEPRREVAEL-NH_2, respectively.

2.1. Human cancer tissue sections and tissue microarrays

Formalin fixed and paraffin embedded (FFPE) human cancer tissue sections (HuCAT446, HuCAT296, and HuCAT396) and human cancer tissue microarrays (TMA) (T262 and T083) were purchased from US Biomax Inc. (Rockville, MD, USA). The human cancer tissue sections include bone (OS of left thigh), breast (infiltrating lobular carcinoma of right breast), and kidney cancers (clear cell carcinoma of right kidney). Bone cancer TMA (T262) contained 12 cases and 24 cores (diameter = 1.5 mm and thickness = 5 μm): OS of left lower limb (OS Limb), OS of right proximal humerus (OS Hum), parosteal OS of skull (OS Skull), osteoblastic OS of left distal femur (OB OS), fibroblastic OS of costal bone (FB OS), telangiectatic OS of left distal femur (TG OS), chondrosarcoma (CS) of humerus (CS Hum), myxoid CS of left femur (MX CS), mesenchymal CS of left leg (Mes CS), CS of right maxilla (CS Max), normal bone tissue (Bone), and normal cartilage tissue (Cartilage). Breast cancer TMA (T083) contained 6 cases and 12 cores: ductal carcinoma (moderately-differentiated or poorly differentiated), lobular carcinoma, apocrine carcinoma, normal breast tissues, and malignant melanoma (tissue marker). The FFPE human cancer tissue sections and TMAs were deparaffinized in 100% xylene, rehydrated with a graded series of alcohols (100, 95, and 80% ethanol in distilled H_2O), and stained with molecular imaging probes (HABPs) or H&E reagents for further histological studies.

2.2. Fluorescence microscopy

Each human cancer tissue section was stained with 2 μM of FITC, cHABP, or HABP-19 at room temperature (RT) for 30 min, washed extensively with PBS to remove unincorporated probes. Fluorescence images were captured using an IX51 microscope (Olympus Corporation, Center Valley, PA) with excitation at 488 nm. FV 1000 Viewer software (Olympus) was used for image analysis.

2.3. Optical imaging of TMAs

For optical imaging, each human cancer TMA was incubated with 2 μM HABP-19 for 30 min and thoroughly washed with PBS to remove unbound probe. Images were acquired using the Maestro 2 optical imaging system (CRi Inc., Woburn, MA). To validate the selective accumulation of imaging probes, a green (FITC) filter set (acquisition setting: 550 to 800 in 10 nm steps and 100 ms exposure time) was used. The fluorescence images obtained were corrected to remove the auto-fluorescence background using the multi-excitation spectral analysis function (Maestro software v. 2.10).

2.4. Cell culture and induction of mineralization

Human osteosarcoma SaOS-2 cells (HTB-85, ATCC, Manassas, VA) were cultured in McCoy's 5A media (ATCC) containing 100 U/mL penicillin, 100 mg/mL streptomycin (both from Sigma-Aldrich Corporation), and 15% fetal bovine serum (FBS, v/v; Gibco) as control media (CM). To enhance SaOS-2 differentiation, cells were grown in control medium supplemented with 50 μg/mL ascorbic acid (AA; Sigma-Aldrich Corporation) and 7.5 mM β-glycerophosphate (β-GP; Sigma-Aldrich Corporation) as stimulating media (SM). The first day of culture in SM for the induction of mineralization was defined as day 0. The culture medium was replaced with a fresh medium every 2 days.

2.5. Quantification of mineralized layer by Alizarin Red S (ARS) staining

Cell monolayer was washed with PBS and fixed in 10% (v/v) formaldehyde at RT for 30 min. The monolayer was then washed twice with excess distilled H_2O prior to an addition of 1 mL of 40 mM ARS (pH 4.2) per well for 30 min. After aspiration of the unincorporated dye, the wells were washed four times with 1 mL H_2O while shaking for 10 min. For corroborative visualization of the extent of mineralization, the stained cells were evaluated by a light microscopy and captured by a digital camera after the unbound ARS was removed by washing. For quantification of ARS staining, 400 μL 10% (v/v) acetic acid was added to each well for 30 min with shaking. The monolayer was then scraped from the plate and transferred with 10% (v/v) acetic acid to a 1.5-mL tube. After vortexing for 30 s, the slurry was overlaid with 250 μL mineral oil, heated to exactly 85 °C for 10 min, and transferred to ice for 5 min. The slurry was then centrifuged at 15,000 *g* for 15 min and 300 μL of the supernatant was removed to a new 1.5-mL tube. Then 200 μL of 10% (v/v) ammonium hydroxide was added to neutralize the acid. Aliquots (100 μL) of the supernatant were read in triplicate at 405 nm in 96-well plate with a SpectraMAX microplate reader (Molecular Devices Corporation).

2.6. Quantification of HA by molecular imaging probes

Each cell monolayer cultured in CM or SM was washed with PBS and stained with 2 μM of HABP-19 at RT for 60 min. The monolayer was then washed extensively with PBS to remove unincorporated probes. Fluorescence images were acquired using the Maestro 2 optical imaging system. Average signal intensity of HABP-19 in the CM and SM was carried out for correlation at indicated time points.

2.7. Statistical analyses

Data were analyzed for statistical significance using Student's *t*-test or single factor ANOVA. Means, standard deviations and degrees of significance are shown on individual data graphs in the 'Results' section. A probability (p) value of <0.05 was considered significant unless otherwise indicated.

3. Results

3.1. Identification of HA in tumor sections

The physicochemical and optical properties of HABP-19 and cHABP were fully characterized previously [23,27]. In our prior study, selective HA binding affinity of a series of probes, FITC, cHABP, and HABP-19, has been studied (Supplementary Fig. S1). Our data indicate that HABP-19 has significant HA binding affinity than cHABP does (>20-fold, $P < 0.005$) and exhibits exceptional HA binding affinity but not with CO (>6-fold, $P < 0.005$).

Although the HA binding affinity results are convincing, HABP-19's capability of recognizing osteotropic cancers associated with HA still needs to be further validated. To determine the HA binding property of aforementioned probes ex vivo, human tumor tissue sections of OS, breast, and kidney cancers were stained with HABP-19 (Fig. 1A). FITC and cHABP were used as negative and positive control, respectively. Background fluorescence of control samples was negligible at the investigated emission window (671–705 nm) (Fig. 1B). No apparent staining signals of both FITC and cHABP were observed in all three tumor sections (Fig. 1C and D). HABP-19 showed abundant binding ability to an OS tissue section, as indicated by strong fluorescence signal, much less binding to a breast, and no binding to a kidney tumor section (Fig. 1E), supporting the observation that Gla residues on HABP-19 play a key role in binding with HA [24–26].

3.2. Detection of HA in tumor tissue microarrays (TMAs)

TMAs have been used as useful methods for the diagnosis and systemic study of a large group of tumors. Evaluating a cohort of osteotropic cancers in one slide is of great value, in which many different osteotropic cancer subtypes are present. Accordingly, we applied the TMA technology to osteotropic cancers, OS and breast cancers, to compare their morphological patterns with the conventional paraffin blocks. HABP-19 staining was performed as outlined in Materials and methods section on OS TMAs consisting of tissue cores of normal or primary tumors collected from 12 people (Fig. 2A) and breast TMAs consisting of tissue cores of normal or primary tumors collected from 6 people (Fig. 2B). In the bright field of optical imaging system, it was almost impossible to identify what cores of OS and breast are HA positive. However, it clearly shows that HABP-19 binding patterns are quite different in the green fluorescence field, indicating that each tumor core in TMA could be categorized into several subtypes according to its expression level to the HABP-19 fluorescence. Several OS cores showed outstanding binding to HABP-19 including OS of lower limb, parosteal OS of skull, fibroblastic OS, telangiectatic OS, and normal bone tissues, as indicated by a strong fluorescence signal, much less binding to osteoblastic OS, and very limited or nonspecific binding to humerus OS and all investigated chondrosarcomas including humerus CS, myxoid CS, mesenchymal CS, maxilla CS, and normal cartilage tissues. In breast cancer TMAs, HABP-19 expressed a strong fluorescence signal to apocrine breast carcinomas, much less signal to lobular carcinomas, and nonspecific binding to ductal carcinomas of moderately-differentiated or poorly differentiated, normal breast tissue, and malignant melanoma tissue markers.

3.3. Microscopic observation of HA calcification in TMAs

Due to the prominent binding property of HABP-19 with the investigated tumor TMA subtypes, we further speculated whether stained H&E patterns in OS and breast cancer TMAs are correlated with the binding patterns of HABP-19 to TMAs observed by a fluorescence microscope (Fig. 3 and Supplementary Fig. S2). As shown in H&E staining images, it was impossible to distinguish calcified areas from the cores of both TMAs. However, HABP-19 clearly showed a strong binding capacity to several subtypes of OS tumors, less strong binding to normal bone tissues, and mostly no binding to chondrosarcoma tumors (Fig. 3A). Similarly, HABP-19 showed relatively strong binding with apocrine breast carcinomas, limited binding with lobular carcinomas, and nonspecific binding to ductal carcinomas, normal breast, and melanoma tissue markers (Fig. 3B).

3.4. Mineralization of SaOS-2 osteosarcoma cells

To evaluate early stage mineralization of osteosarcoma cancers in vitro, human osteosarcoma (SaOS-2) cells were cultured in control media (CM) or stimulating media (SM) supplemented with ascorbic acid (AA) and β-glycerophosphate (β-GP), which are well known osteogenic factors that stimulate osteoblastic differentiation and mineralization [28–30]. The cultured cells were stained with Alizarin Red S (ARS) and quantified by absorbance spectroscopy (Fig. 4A and B). As expected, the detected mineral deposition was highly enhanced by the addition of SM (e.g., AA and β-GP) in SaOS-2 cell cultures (Fig. 4A). The effect of CM and SM in producing mineral depositions was not significant at day 4. Therefore, the effects of extrinsic osteogenic factors are not a crucial factor in influencing the biological activity of SaOS-2 cells in an early time point. However, the stimulated (SM) SaOS-2 cells produced significant amount of calcium minerals (3.02 ± 0.4 mM) compared to non-stimulated (CM) cells at day 8 (0.19 ± 0.01 mM, $P < 0.05$) and at day 12 (0.43 ± 0.04 mM, $P < 0.05$) (Fig. 4B).

To determine HA calcification on the mineralized monolayer based on the above ARS results, SaOS-2 cells cultured in CM or SM were stained with HABP-19, visualized, and

quantified by optical imaging system (Fig. 4C and D). Fluorescence signal (white pseudo color) was dramatically increased in the SM treated cells at day 12, whereas minimal signal intensity in the CM treated cells was observed both at days 8 and 12 (Fig. 4C). SM treated cells have expressed outstanding signal intensities at days 8 (54.35 ± 22.81) and 12 (164.92 ± 28.93). However, CM treated cells did not show any significant HA deposition at any time point (Fig. 4D).

4. Discussion

Although OSs are aggressive neoplasms with a wide range of morphological patterns, early detection with high sensitivity and specificity would greatly improve treatment and patient survival. Consequently, reliable biomarkers that could identify early stage diagnosis of malignant tumor cells, capable of producing HA calcification, and would help distinguish HA from other elements in osteotropic cancers are crucial for a more effective treatment of OS patients at an early stage. Protein OCN is a sensitive and specific marker for bone cells and may play a crucial role in identifying a bone-forming tumor such as OS. The current study therefore focused on developing protein OCN derived biomarkers. We are able to detect HA calcification with high sensitivity and specificity by applying an OCN inspired biomimetic to osteotropic cancers ex vivo and SaOS-2 cells in vitro. The specificity was supported by limited cHABP binding to osteotropic tumors and completely blocked HABP-19 binding to kidney tumors.

CO calcifications are mainly seen in benign tumors and kidney stones, hard crystalline mineral deposits formed within the kidney or urinary tract, whereas HA calcifications can be found in both benign and malignant lesions [24–26]. Evidence of an effect of kidney stones to increase kidney cancer risk remains mixed. A cohort study showed a 150% risk increase for cancers of the renal pelvis in people hospitalized for kidney stones [31]. The tumors mainly developed on the same side as the stone, and it was hypothesized that chronic irritation and infections related to the stone were the cause of the increased kidney cancer risk. However, an earlier case–control study showed no risk increase for cancers of the renal pelvis in people with a history of kidney stones [32]. Although pathological relationships between kidney stones and kidney cancers are mostly unknown, it seems that renal cell carcinoma in this study does not contain HA or CO component because their expression to the HABP-19 was negative.

Since it is hard to distinguish the varied histological subtypes of OS, their diagnosis may be difficult and problematic. Their differential diagnoses can include many tumors, such as other subtypes of sarcomas, carcinoma, lymphoma, or even melanoma. Therefore, we introduced tissue microarrays to identify different subtypes of osteotropic cancers in OS and breast cancers based on the binding pattern of individual core with HABP-19. Most OS subtypes and apocrine breast carcinomas showed outstanding HABP-19 binding property with strong fluorescence signals, while most chondrosarcoma subtypes, lobular carcinomas, and ductal carcinomas did not express noticeable HABP-19 signals. OS tumors were originally misdiagnosed because of a lack of identifiable osteoid or bone [33,34]. Different subtypes of OSs may produce heterogeneous matrices including bone, cartilage, and collagen, which are difficult to distinguish from the neoplastic bone. It has been suggested that CO calcifications are a product of secretions, whereas HA calcifications result from cellular degradation or necrosis [25,35]. While HA is largely known for its role in conferring structural and mechanical properties to bone, it also functions as a bioactive material that directly regulates the behavior of both normal and malignant tumor cells [36–38]. Nevertheless, it is not clear whether HA directly affects the pathogenesis of bone diseases and bone metastasis.

Human SaOS-2 cells used as a model of mineralizing cells activated osteogenic activity in SM as seen in the enhanced HA nodule formation and cell differentiation compared to cells that had been grown on CM. Significantly increased HA deposition was also observed in SaOS-2 cells grown on SM. Our findings are consistent with earlier reports on osteoblast differentiation induced by a concomitant addition of AA and β-GP [28,29]. The pattern of HA deposits in SM treated cells shown in optical imaging analysis was similar with the trend of mineralization shown in the ARS results. In CM cultures, the observed HA monolayer was not significant, even though SaOS-2 cells produced distinguishable mineral deposition at day 12 compared to other investigated time points ($P < 0.05$), indicating that normal cell culture condition (CM) may play a role in mineral formation but not in HA calcification of SaOS-2 cells. It is interesting to speculate how OS cells could form HA calcification in vitro and in vivo. SaOS-2 cells are able to induce HA crystal deposits during mineralization in vitro suggesting that they can generate a microenvironment that favors the crystallization of calcium and phosphate ions into HA.

Although Raman spectroscopy has been applied to distinguish two types of microcalcifications occurring in benign and malignant lesions, it is unclear whether the Raman spectroscopic method is suitable for distinguishing microcalcifications in vivo [39,40]. Currently, a variety of imaging modalities and spectroscopic techniques are being explored to improve osteotropic cancer diagnosis and treatment [41–44]. However, there is no reliable diagnostic imaging marker or medical modality to distinguish accurately between CO and HA calcifications with high affinity and specificity in biological tissues non-invasively. Even the most advanced clinical imaging modalities, such as optical coherence tomography, magnetic resonance imaging (MRI), and ultrasonography, have difficulty distinguishing them. Without a reliable analytical method, a clear correlation between HA calcification and osteotropic cancers cannot be obtained. We have previously shown that HABP-19 has high affinity and specificity for HA. This specificity is illustrated by the ability of HABP-19 to image HA, but not CO, calcifications in the SaOS-2 osteosarcoma model presented in this study. Our HABP-19 may be quite useful in developing contrast agents for dual-imaging modalities, MRI, positron emission tomography (PET), or single-photon emission computed tomography (SPECT), by introducing near infrared (NIR) fluorescence. It is possible to extend our fluorescence approach to other imaging modalities by conjugating NIR fluorescence and HABP-19 to DOTA (1,4,7,10-tetraazacyclododecane-1,4,7,10-tetraacetic acid), which is a high affinity chelating agent especially for Gd^{3+}, ^{111}In, and ^{68}Ga among others. These conjugates should have high specificity for HA and sufficient relaxivity to produce MRI/NIR, PET/NIR, or SPECT/NIR dual-modality contrast agents.

Fluorescence imaging technology has been widely used in preclinical study of cancers [45–50]. For example, fluorescent proteins of different colors used to color-code OS cancer cells of a specific genotype or phenotype were applied to study tumor development [47–50]. In one study, it was described that the interaction of highly metastatic GFP-labeled 143B OS cancer cells and low metastatic RFP-labeled MNNG/HOS cells can be directly compared in vivo in the same tumor, demonstrating the capability of color-coded imaging for visualizing different metastatic potential and cancer-cell/cancer-cell interactions within the mixed tumor in vivo [50]. It could be even more informative by including a fluorescently labeled HABP-19 which has a different color. Real-time multicolor imaging of fluorescent proteins and fluorescent HABP-19 will be especially useful to study the complex process of osteotropic cancer development and tumor metastasis in mouse model.

In summary, we have shown that it is possible to selectively image HA in osteotropic cancers ex vivo and in human SaOS-2 cells in vitro by using HABP-19. A variety of

multimodal biomarkers based on HABP-19 can be tested in a straightforward and reliable osteotropic cancer animal model system.

Supplementary Material

Refer to Web version on PubMed Central for supplementary material.

Acknowledgments

The authors thank Dr. Yoo-Shin Kim, Dr. David Choi, and Dr. Wael R. Abd-Elgaliel for technical supports and comments (The Methodist Hospital Research Institute).

Grant support: This research was supported by NIH CA135312.

Abbreviations

HA	hydroxyapatite
HABP	hydroxyapatite binding peptide
OCN	osteocalcin
OS	osteosarcoma
Gla	γ-carboxyglutamic acid
CO	calcium oxalate
TMA	tissue microarray
FB	fibroblastic
TG	telangiectatic
CS	chondrosarcoma
MX	myxoid
Max	maxilla
β-GP	β-Glycerophosphate
ARS	Alizarin Red S
CM	control media
SM	stimulating media

References

1. Fuchs B, Pritchard DJ. Etiology of osteosarcoma. Clin Orthop Relat Res. 2002; 397:40–52. [PubMed: 11953594]
2. Mercadante S. Malignant bone pain: pathophysiology and treatment. Pain. 1997; 69:1–18. [PubMed: 9060007]
3. Kager L, Zoubek A, Potschger U, Kastner U, Flege S, Kempf-Bielack B, Branscheid D, Kotz R, Salzer-Kuntschik M, Winkelmann W, Jundt G, Kabisch H, Reichardt P, Jurgens H, Gadner H, Bielack SS. Primary metastatic osteosarcoma: presentation and outcome of patients treated on neoadjuvant Cooperative Osteosarcoma Study Group protocols. J Clin Oncol. 2003; 21:2011–2018. [PubMed: 12743156]
4. DuBois S, Demetri G. Markers of angiogenesis and clinical features in patients with sarcoma. Cancer. 2007; 109:813–819. [PubMed: 17265525]
5. Kansara M, Thomas DM. Molecular pathogenesis of osteosarcoma. DNA Cell Biol. 2007; 26:1–18. [PubMed: 17263592]

6. Scotlandi K, Picci P, Kovar H. Targeted therapies in bone sarcomas. Curr Cancer Drug Targets. 2009; 9:843–853. [PubMed: 20025572]
7. Ottaviani G, Jaffe N. The epidemiology of osteosarcoma. Cancer Treat Res. 2009; 152:3–13. [PubMed: 20213383]
8. Mialou V, Philip T, Kalifa C, Perol D, Gentet JC, Marec-Berard P, Pacquement H, Chastagner P, Defaschelles AS, Hartmann O. Metastatic osteosarcoma at diagnosis: prognostic factors and long-term outcome — the French pediatric experience. Cancer. 2005; 104:1100–1109. [PubMed: 16015627]
9. Picci P. Osteosarcoma (osteogenic sarcoma). Orphanet J Rare Dis. 2007; 2:6. [PubMed: 17244349]
10. Wittig JC, Bickels J, Priebat D, Jelinek J, Kellar-Graney K, Shmookler B, Malawer MM. Osteosarcoma: a multidisciplinary approach to diagnosis and treatment. Am Fam Physician. 2002; 65:1123–1132. [PubMed: 11925089]
11. Sabile AA, Arlt MJE, Muff R, Bode B, Langsam B, Bertz J, Jentzsch T, Puskas GJ, Born W, Fuchs B. Cyr61 expression in osteosarcoma indicates poor prognosis and promotes intratibial growth and lung metastasis in mice. J Bone Miner Res. 2012; 27:58–67. [PubMed: 21976359]
12. Shehadeh AM, Haiba MA, Henshaw RM, Lack E. Telangiectatic osteosarcoma of the patella. Orthopedics. 2008; 31:808. [PubMed: 19292411]
13. Fanburg-Smith JC, Bratthauer GL, Miettinen M. Osteocalcin and osteonectin immunoreactivity in extraskeletal osteosarcoma: a study of 28 cases. Hum Pathol. 1999; 30:32–38. [PubMed: 9923924]
14. Koeneman KS, Kao C, Ko SC, Yang L, Wada Y, Kallmes DF, Gillenwater JY, Zhau HE, Chung LW, Gardner TA. Osteocalcin-directed gene therapy for prostate-cancer bone metastasis. World J Urol. 2000; 18:102–110. [PubMed: 10854144]
15. Johnson NA, Chen BH, Sung SY, Liao CH, Hsiao WC, Chung LWK, Hsieh CL. A novel targeting modality for renal cell carcinoma: human osteocalcin promoter-mediated gene therapy synergistically induced by vitamin C and vitamin D(3). J Gene Med. 2010; 12:892–903. [PubMed: 21105150]
16. Hauschka PV, Wians FH Jr. Osteocalcin-hydroxyapatite interaction in the extracellular organic matrix of bone. Anat Rec. 1989; 224:180–188. [PubMed: 2549810]
17. Hoang QQ, Sicheri F, Howard AJ, Yang DSC. Bone recognition mechanism of porcine osteocalcin from crystal structure. Nature. 2003; 425:977–980. [PubMed: 14586470]
18. Bellahcene A, Castronovo V. Expression of bone matrix proteins in human breast cancer: potential roles in microcalcification formation and in the genesis of bone metastases. Bull Cancer. 1997; 84:17–24. [PubMed: 9180854]
19. Bandyopadhyay PK, Garrett JE, Shetty RP, Keate T, Walker CS, BM. gamma-Glutamyl carboxylation: An extracellular posttranslational modification that antedates the divergence of molluscs, arthropods, and chordates. Proc Natl Acad Sci U S A. 2002; 99:1264–1269. [PubMed: 11818531]
20. Luo G, Ducy P, McKee MD, Pinero GJ, Loyer E, Behringer RR, Karsenty G. Spontaneous calcification of arteries and cartilage in mice lacking matrix GLA protein. Nature. 1997; 386:78–81. [PubMed: 9052783]
21. Morgan MP, Cooke MM, Christopherson PA, Westfall PR, McCarthy GM. Calcium hydroxyapatite promotes mitogenesis and matrix metalloproteinase expression in human breast cancer cell lines. Mol Carcinog. 2001; 32:111–117. [PubMed: 11746823]
22. Morgan MP, Cooke MM, McCarthy GM. Microcalcifications associated with breast cancer: an epiphenomenon or biologically significant feature of selected tumors? J Mammary Gland Biol Neoplasia. 2005; 10:181–187. [PubMed: 16025224]
23. Lee JS, Morrisett JD, Tung CH. Detection of hydroxyapatite in calcified cardiovascular tissues. Atherosclerosis. 2012; 224:340–347. [PubMed: 22877867]
24. Frappart L, Boudeulle M, Boumendil J, Lin HC, Martinon I, Palayer C, Mallet-Guy Y, Raudrant D, Bremond A, Rochet Y, et al. Structure and composition of microcalcifications in benign and malignant lesions of the breast: study by light microscopy, transmission and scanning electron microscopy, microprobe analysis, and X-ray diffraction. Hum Pathol. 1984; 15:880–889. [PubMed: 6469237]

25. Gonzalez JE, Caldwell RG, Valaitis J. Calcium oxalate crystals in the breast. Pathology and significance. Am J Surg Pathol. 1991; 15:586–591. [PubMed: 2031531]
26. Frappart L, Remy I, Lin HC, Bremond A, Raudrant D, Grousson B, Vauzelle JL. Different types of microcalcifications observed in breast pathology. Correlations with histopathological diagnosis and radiological examination of operative specimens. Virchows Arch A Pathol Anat Histopathol. 1986; 410:179–187. [PubMed: 3026082]
27. Lee JS, Tung CH. Osteocalcin biomimic recognizes bone hydroxyapatite. Chem Bio Chem. 2011; 12:1669–1673.
28. Gillette JM, Nielsen-Preiss SM. The role of annexin 2 in osteoblastic mineralization. J Cell Sci. 2004; 117:441–449. [PubMed: 14679310]
29. Vaingankar SM, Fitzpatrick TA, Johnson K, Goding JW, Maurice M, Terkeltaub R. Subcellular targeting and function of osteoblast nucleotide pyrophosphatase phosphodiesterase 1. Am J Physiol Cell Physiol. 2004; 286:C1177–1187. [PubMed: 15075217]
30. Thouverey C, Strzelecka-Kiliszek A, Balcerzak M, Buchet R, Pikula S. Matrix vesicles originate from apical membrane microvilli of mineralizing osteoblast-like Saos-2 cells. J Cell Biochem. 2009; 106:127–138. [PubMed: 19009559]
31. Chow WH, Lindblad P, Gridley G, Nyren O, McLaughlin JK, Linet MS, Pennello GA, Adami HO, Fraumeni JF Jr. Risk of urinary tract cancers following kidney or ureter stones. J Natl Cancer Inst. 1997; 89:1453–1457. [PubMed: 9326915]
32. Liaw KL, Linet MS, McLaughlin JK, Yu MC, Schoenberg JB, Lynch CF, Niwa S, Fraumeni JF Jr. Possible relation between hypertension and cancers of the renal pelvis and ureter. Int J Cancer. 1997; 70:265–268. [PubMed: 9033625]
33. Bane BL, Evans HL, Ro JY, Carrasco CH, Grignon DJ, Benjamin RS, Ayala AG. Extraskeletal osteosarcoma. A clinicopathologic review of 26 cases. Cancer. 1990; 65:2762–2770. [PubMed: 2160317]
34. Young RH, Rosenberg AE. Osteosarcoma of the urinary bladder. Report of a case and review of the literature. Cancer. 1987; 59:174–178. [PubMed: 3466661]
35. Castronovo V, Bellahcene A. Evidence that breast cancer associated microcalcifications are mineralized malignant cells. Int J Oncol. 1998; 12:305–308. [PubMed: 9458353]
36. Lee JS, Lee JS, Wagoner-Johnson A, Murphy WL. Modular peptide growth factors for substrate-mediated stem cell differentiation. Angew Chem Int Ed Engl. 2009; 48:6266–6269. [PubMed: 19610001]
37. Lee JS, Lee JS, Murphy WL. Modular peptides promote human mesenchymal stem cell differentiation on biomaterial surfaces. Acta Biomater. 2010; 6:21–28. [PubMed: 19665062]
38. Pathi SP, Kowalczewski C, Tadipatri R, Fischbach C. A novel 3-D mineralized tumor model to study breast cancer bone metastasis. PLoS ONE. 2010; 5:e8849. [PubMed: 20107512]
39. Haka AS, Shafer-Peltier KE, Fitzmaurice M, Crowe J, Dasari RR, Feld MS. Identifying microcalcifications in benign and malignant breast lesions by probing differences in their chemical composition using Raman spectroscopy. Cancer Res. 2002; 62:5375–5380. [PubMed: 12235010]
40. Haka AS, Volynskaya Z, Gardecki JA, Nazemi J, Shenk R, Wang N, Dasari RR, Fitzmaurice M, Feld MS. Diagnosing breast cancer using Raman spectroscopy: prospective analysis. J Biomed Opt. 2009; 14:054023. [PubMed: 19895125]
41. Dutour A, Leclers D, Monteil J, Paraf F, Charissoux JL, Rousseau R, Rigaud M. Non-invasive imaging correlates with histological and molecular characteristics of an osteosarcoma model: application for early detection and follow-up of MDR phenotype. Anticancer Res. 2007; 27:4171–4178. [PubMed: 18225588]
42. Lenkinski RE, Ahmed M, Zaheer A, Frangioni JV, Goldberg SN. Near-infrared fluorescence imaging of microcalcification in an animal model of breast cancer. Acad Radiol. 2003; 10:1159–1164. [PubMed: 14587634]
43. Sun X, Niu G, Yan Y, Yang M, Chen K, Ma Y, Chan N, Shen B, Chen X. Phage display-derived peptides for osteosarcoma imaging. Clin Cancer Res. 2010; 16:4268–4277. [PubMed: 20570932]
44. Bhushan KR, Misra P, Liu F, Mathur S, Lenkinski RE, Frangioni JV. Detection of breast cancer microcalcifications using a dual-modality SPECT/NIR fluorescent probe. J Am Chem Soc. 2008; 130:17648–17649. [PubMed: 19055348]

45. Weissleder R, Tung CH, Mahmood U, Bogdanov A Jr. In vivo imaging of tumors with protease-activated near-infrared fluorescent probes. Nat Biotechnol. 1999; 17:375–378. [PubMed: 10207887]

46. Bremer C, Tung CH, Weissleder R. In vivo molecular target assessment of matrix metalloproteinase inhibition. Nat Med. 2001; 7:743–748. [PubMed: 11385514]

47. Chishima T, Miyagi Y, Wang X, Yamaoka H, Shimada H, Moossa AR, Hoffman RM. Cancer invasion and micrometastasis visualized in live tissue by green fluorescent protein expression. Cancer Res. 1997; 57:2042–2047. [PubMed: 9158003]

48. Hoffman RM. The multiple uses of fluorescent proteins to visualize cancer in Olivera, vivo. Nat Rev Cancer. 2005; 5:796–806. [PubMed: 16195751]

49. Hayashi K, Zhao M, Yamauchi K, Yamamoto N, Tsuchiya H, Tomita K, Kishimoto H, Bouvet M, Hoffman RM. Systemic targeting of primary bone tumor and lung metastasis of high-grade osteosarcoma in nude mice with a tumor-selective strain of *Salmonella typhimurium*. Cell Cycle. 2009; 8:870–875. [PubMed: 19221501]

50. Tome Y, Tsuchiya H, Hayashi K, Yamauchi K, Sugimoto N, Kanaya F, Tomita K, Hoffman RM. In vivo gene transfer between interacting human osteosarcoma cell lines is associated with acquisition of enhanced metastatic potential. J Cell Biochem. 2009; 108:362–367. [PubMed: 19623575]

Appendix A. Supplementary data

Supplementary data to this article can be found online at http://dx.doi.org/10.1016/j.bbagen.2013.05.015.

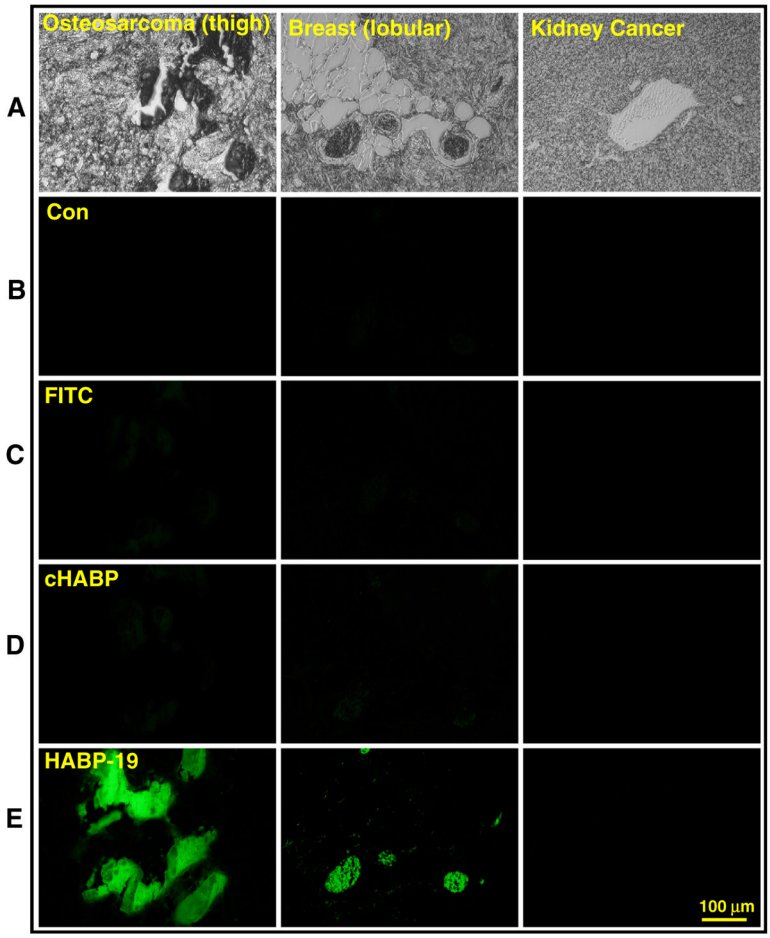

Fig. 1.

Histology of tumor sections stained with molecular imaging biomarkers. (A) Bright field images of sectioned cancer tissues. (B) Auto-fluorescence of tumors incubated in PBS. Human cancer tissue sections were stained with 2 μM of (C) FITC, (D) cHABP, or (E) HABP-19 for 30 min, washed extensively with PBS to remove unincorporated biomarkers. Fluorescence images were observed by fluorescence microscopy to detect bound HA calcification on tissue sections.

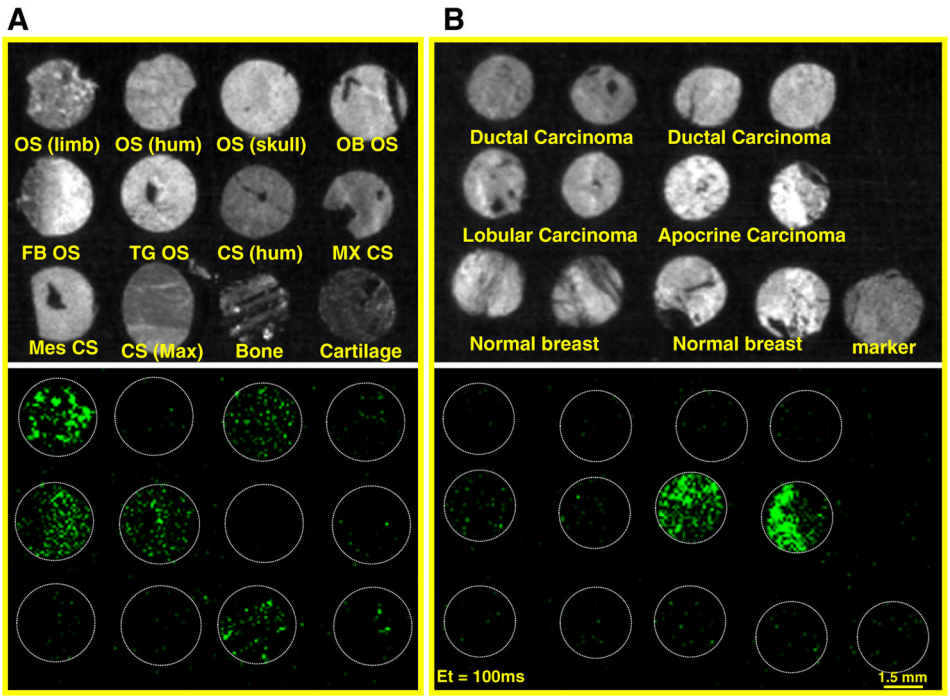

Fig. 2.

Optical molecular images of tumor tissue microarrays (TMAs). Bright field image (top) and fluorescent image (bottom) of osteosarcomas (A) and breast cancers (B). TMAs incubated with HABP-19 were thoroughly washed with PBS to remove any unbound probe. Optical molecular images were acquired using a Maestro 2 optical imaging system with a 100 ms exposure time. To validate the selective binding of HABP-19 on TMAs, a green filter set was used (acquisition setting: 550 to 800 in 10-nm steps). Bone cancer TMA (T262) contained 12 cases and 24 cores (diameter = 1.5 mm and thickness = 5 μm): OS of left lower limb (OS Limb), OS of right proximal humerus (OS Hum), parosteal OS of skull (OS Skull), osteoblastic OS of left distal femur (OB OS), fibroblastic OS of costal bone (FB OS), telangiectatic OS of left distal femur (TG OS), chondrosarcoma (CS) of humerus (CS Hum), myxoid CS of left femur (MX CS), mesenchymal CS of left leg (Mes CS), CS of right maxilla (CS Max), normal bone tissue (Bone), and normal cartilage tissue (Cartilage). Breast cancer TMA (T083) contained 6 cases and 12 cores: ductal (moderately-differentiated or poorly differentiated), lobular, apocrine carcinoma, normal breast tissues, and malignant melanoma (tissue marker).

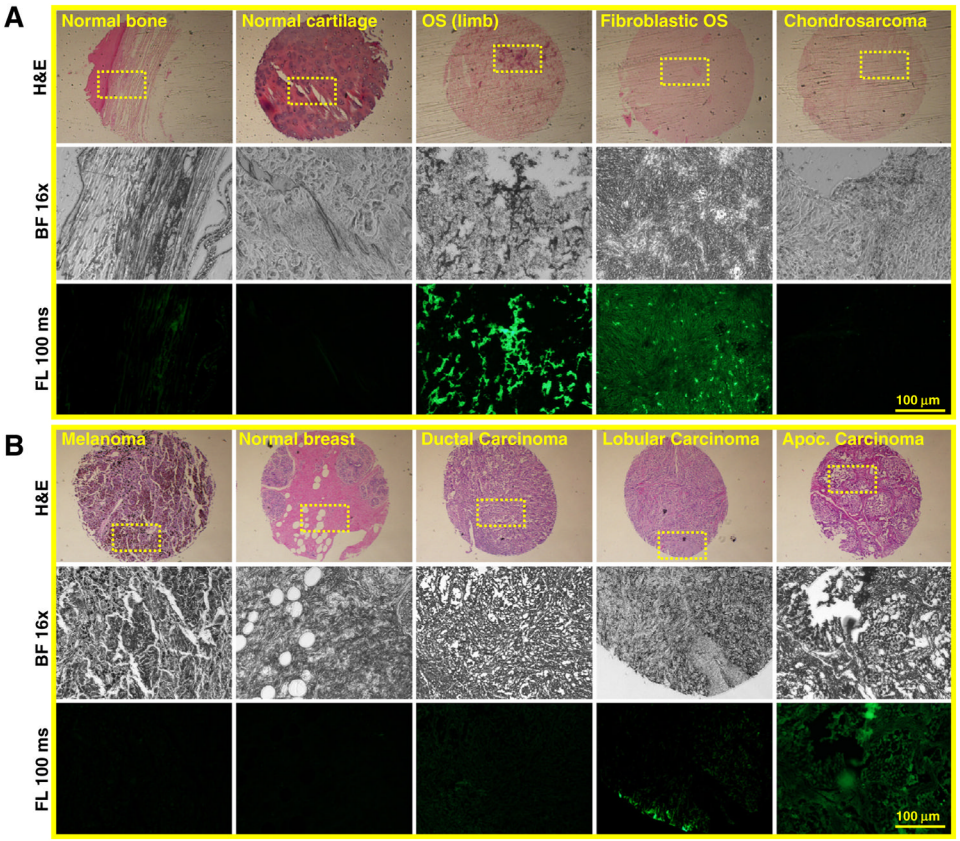

Fig. 3.

Histological analysis of Tumor TMAs. (A) Subtypes of OS TMAs were stained with H&E (top) or HABP-19 (bottom) to identify HA calcification. (B) Subtypes of breast cancer TMAs were stained with H&E (top) or HABP-19 (bottom) to detect HA calcification. The yellow dot rectangle was magnified in the bright field (middle) and fluorescence field view (bottom). More images can be found at Supplementary Fig. S2.

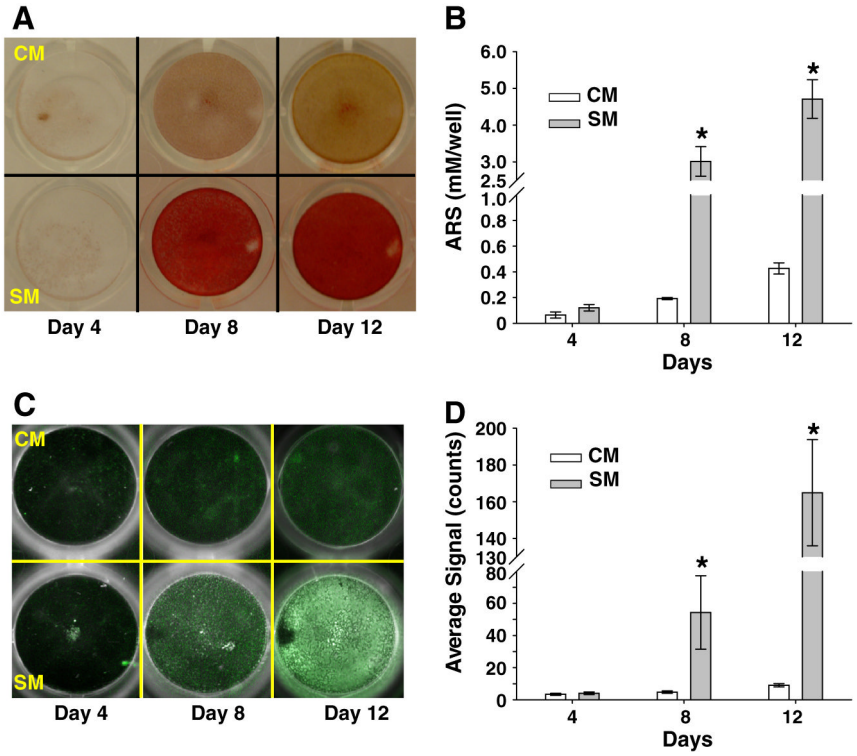

Fig. 4.

Identification of mineral layer and HA calcification induced by SaOS-2 cells. Cells were incubated under control medium (CM) or stimulating medium (SM) supplemented with 50 μg/mL ascorbic acid (AA) and 7.5 mM β-glycerophosphate (β-GP) for the indicated time points. (A) Cells cultured in CM or SM were stained with Alizarin Red-S (ARS) to detect calcium mineral layer and captured by a digital camera after removal of unbound ARS dye by washing. (B) Mineral layers stained with ARS in CM or SM culture were quantified at 405 nm (results are mean ± SD, n = 4). (C) HA deposits induced by SaOS-2 cells during CM or SM cultures were stained with HABP-19 at the indicated time points and visualized by a Maestro optical molecular imaging system. The acquired images are shown as pseudo color-enhanced fluorescence superimposed on the white light images. (D) Region of interest (ROI) covering each culture plate well was used to quantify average signal intensity of HABP-19 (results are mean ± SD, n = 4). Significantly different P value ($P < 0.05$) between CM and SM was indicated as asterisk (*).